A Consumer-Oriented Control Framework for Performance Analysis in Hybrid Electric Vehicles

Mohamed L. Shaltout, *Member, IEEE*, Andreas A. Malikopoulos, *Member, IEEE*, Sreekanth Pannala, and Dongmei Chen, *Member, IEEE*

***Abstract*— Hybrid electric vehicles (HEVs) have attracted considerable attention due to their potential to reduce fuel consumption and emissions. The objective of this paper is to enhance our understanding of the associated tradeoffs among the HEV subsystems, e.g., the engine, the motor, and the battery, and investigate the related implications for fuel consumption and battery capacity and lifetime. Addressing this problem can provide insights on how to prioritize these objectives based on consumers' needs and preferences. The results of the proposed optimization approach can also be used to investigate the implications for HEV costs related to ownership and warranty.**

***Index Terms*— Battery capacity and lifetime, hybrid electric vehicles (HEVs), multiobjective optimization, power management control.**

I. Introduction

A. Motivation

WIDESPREAD use of various hybrid powertrains is inevitable and many opportunities for substantial progress remain. Hybrid electric vehicles (HEVs) and plug-in HEVs (PHEVs) have held great intuitive appeal and have attracted considerable attention due to their potential to reduce petroleum consumption and greenhouse gas (GHG) emissions. The main advantage of HEVs and PHEVs is the existence of individual subsystems, e.g., the internal combustion engine, the electric machines (motor and generator), and the energy storage system (battery) that can power the vehicle either separately or in combination. The supervisory power management control algorithm determines how to distribute the power demanded by the driver to these subsystems. Traditionally, maximizing fuel economy and minimizing GHG emissions are the main objectives of the control development. With the introduction of batteries, prolonging the battery life is considered highly important during the control design from the consumer's perspective due to associated ownership and warranty costs. Thus, it is necessary to develop a control framework for vehicle power management that will be able to balance maximum fuel economy, minimum GHG emissions, and extended battery life based on consumer's needs and preferences.

Manuscript received April 3, 2014; revised August 29, 2014; accepted November 1, 2014. Date of publication December 9, 2014; date of current version June 12, 2015. Manuscript received in final form November 23, 2014. This work was supported in part by the Laboratory Directed Research and Development Program through the Oak Ridge National Laboratory, Oak Ridge, TN, USA, managed by UTBattelle, LLC, for Department of Energy (DOE), and in part by the UTBattelle, LLC, through the U.S. DOE under Contract DE-AC05-00OR22725. Recommended by Associate Editor K. Butts.

M. L. Shaltout and D. Chen are with the Department of Mechanical Engineering, University of Texas at Austin, Austin, TX 78712 USA (e-mail: mshaltout@utexas.edu; dmchen@me.utexas.edu).

A. A. Malikopoulos is with the Energy and Transportation Science Division, Oak Ridge National Laboratory, Oak Ridge, TN 37831 USA (e-mail: andreas@ornl.gov).

S. Pannala is with the Computer Science and Mathematics Division, Oak Ridge National Laboratory, Oak Ridge, TN 37831 USA (e-mail: pannalas@ornl.gov).

Color versions of one or more of the figures in this paper are available online at http://ieeexplore.ieee.org.

Digital Object Identifier 10.1109/TCST.2014.2376472

B. Literature Review

A significant amount of work has been conducted on developing online power management algorithms for parallel HEV configurations [1]–[5]. The main aspects of these algorithms are concerned with the self-sustainability of the electrical path, which must be guaranteed for the entire driving cycle, and the fact that limited knowledge of the future driving conditions is available. Such algorithms consist of an instantaneous optimization problem that accounts for storage system state of charge (SoC) variation through the equivalent fuel consumption. The latter is evaluated by considering average energy paths leading from the fuel to the energy storage of the electrical path.

Other research efforts have focused on benchmarking the fuel economy in HEVs by providing the maximum theoretical efficiency they can achieve over a given vehicle speed profile, e.g., driving cycle, using the deterministic formulation of dynamic programming (DP) [6], [7]. DP has also been extended to a stochastic formulation capable of deriving an optimal control policy for a family of driving cycles [8]–[11]. There has also been a significant amount of work using model predictive control (MPC) [12] to address this problem (for a complete list of references on MPC see [13] and the references there).

Although the aforementioned work has aimed at enhancing our understanding of power management control optimization problem in HEVs, the battery system was considered as a free buffer that could be used to either store or use energy

1063-6536 © 2014 IEEE. Personal use is permitted, but republication/redistribution requires IEEE permission.
See http://www.ieee.org/publications_standards/publications/rights/index.html for more information.

at any time. However, the battery's capacity and lifetime have significant implications not only in the overall cost of HEV/PHEV ownership but also in safety, durability, and reliability. Recent research efforts have considered both design and control optimization approaches that include various battery metrics, e.g., capacity, lifetime, and safety, in the objective function. The necessity of developing advanced battery management systems was addressed in [14]. Wang and Cassandras [15] studied the problem of optimally controlling the charge and discharge rate of multiple nonideal batteries to maximize the minimum residual energy of the batteries at the end of a given time period. It was shown the optimal solution is a bang–bang type, with the battery always in recharging mode during the last part of the interval [16].

Some studies have focused on the optimal design of HEVs/PHEVs with respect to the various components. Wang *et al.* [17] proposed an approach to improve the fuel economy and battery lifetime for EVs and parallel PHEVs with a combination of an ultracapacitor and an energy-dense lithium ion battery. Moura *et al.* [18] explored the quantification of the tradeoffs between power management algorithm design and battery energy capacity. The implications of motor/generator and battery size on fuel economy and GHG emissions in a medium-duty PHEV were discussed in [19]. An optimization framework was developed to facilitate better understanding of the potential benefits of proper selection of motor/generator and battery sizes. This understanding can contribute to appropriate sizing of these components, which can have significant impacts on overall PHEV cost.

Lee *et al.* [20] investigated the impact of advanced battery control strategies on the battery size and fuel economy for heavy-duty military HEVs. The objective of these control strategies is to ensure safe and robust operation covering infrequent extreme conditions. Excessive battery operation is moderated by adjusting the battery power upper and lower limits using the feedback of electrode-averaged lithium ion concentration estimated by an extended Kalman filter. Bashash *et al.* [21] investigated simultaneously the minimization of battery degradation and fuel/electricity costs via a multiobjective optimization problem consisting of the total cost of fuel and electricity and the total battery health degradation over a 24 h naturalistic driving cycle. The result of this optimization process is a family of optimal solutions in the form of a Pareto frontier showing the balance between total energy cost and battery resistance growth.

More recently, there has been an effort to develop power management control algorithms for HEVs/PHEVs by also including the battery's lifetime. Serrao *et al.* [22] formulated the power management control problem in HEVs by incorporating the aging of the battery. To explicitly quantify the battery aging, a model that correlates aging with SoC and charge/discharge rates was used. In the objective function of the problem formulation, fuel consumption and battery aging were considered, and the control problem was solved using Pontryagin's minimum principle for three different cases: 1) including only fuel consumption; 2) assigning the weight factor to be 65% for fuel consumption and 35% for battery aging; and 3) assigning the weight factor to be 50% for each objective. In this analysis, the authors found that there is a significant tradeoff between fuel consumption and battery aging. Ebbesen *et al.* [23] presented a power management control algorithm for a parallel HEV by modifying the equivalent consumption minimization strategy to include the battery state of the health in addition to fuel consumption. In this paper, a standard quasi-static backward model was simulated over the Federal Test Procedure (FTP-72) and common Artemis driving cycles and it was found that there is a tradeoff between fuel economy and battery's lifetime. The battery end of life was considered to be when the battery capacity had dropped by 20% from its initial value.

A survey of the supervisory power management control algorithms that have been reported in the literature to date can be found in [24].

C. Contribution of This Paper

The objective of this paper and related research of the authors [25] is to enhance our understanding of the associated tradeoffs among the HEV subsystems, e.g., the engine, the motor, and the battery. Addressing these tradeoffs and related implications in fuel consumption, motor efficiency, and battery capacity and lifetime can aid in developing power management control algorithms that prioritize these objectives based on consumer needs and preferences.

In our analysis, battery temperature is considered as a critical parameter and controlled indirectly throughout the charge/discharge process. Temperature not only plays an important role in safety but also affects the capacity fade as well as life of a battery [26], [27]. The side reactions that enable the growth of solid electrolyte interface and increase the impedance of the cell depend exponentially on temperature through Arrhenius relationship. This leads to rapid irreversible capacity loss and affect the lifetime of the battery. In addition, higher operating temperatures put the battery closer to the flash point of the electrolyte, and thus reduce the margin for safety. For this reason, we have implicitly included temperature in our proposed optimization framework by controlling SoC.

The contributions of this paper are: 1) the development of a multiobjective optimization framework that includes fuel consumption, motor efficiency, and the charge/discharge process—to indirectly address battery use and lifetime—and 2) the implementation of a power management control algorithm yielding the Pareto optimal solution of the multiobjective optimization problem that minimizes the long-run expected average cost criterion in the stochastic control problem formulation.

D. Organization of This Paper

The remainder of this paper proceeds as follows. In Section II, we present the battery and vehicle model used in our analysis. In Section III, we formulate the power management control problem formulation, and in Section IV, we introduce the multiobjective optimization framework and the Pareto control policy. In Section V, we present simulation results and discuss the associated tradeoffs among the subsystems. Finally, in Section VI, we present concluding remarks.

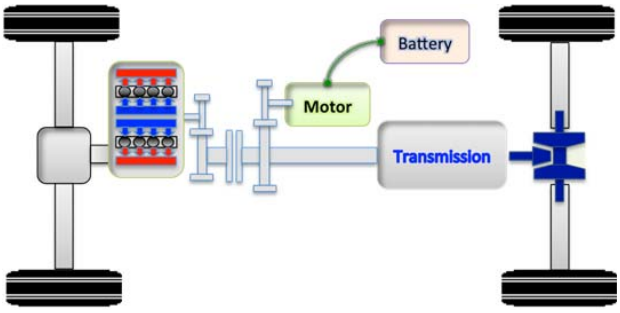

Fig. 1. Schematic of the pretransmission parallel HEV configuration.

TABLE I
PARALLEL HEV SPECIFICATIONS

Vehicle Specifications	
Weight	1,680 kg
Frontal Area	2.2508 m^2
Engine Specifications	
Configuration	4-Cylinder
Displacement	2.2 Liters
Power	110 kW
Transmission Specifications	
Configuration	Automatic
1^{st} Gear Ratio	2.563
2^{nd} Gear Ratio	1.552
3^{rd} Gear Ratio	1.022
4^{th} Gear Ratio	0.727
5^{th} Gear Ratio	0.52
Electric Machine Specifications	
Configuration	Permanent magnet
Peak Power	50 kW
Continuous Power	25 kW
Final Drive Specifications	
Ratio	4.438
Battery Specifications	
Technology	Cylindrical NIMH
Cell Designation	Panasonic HHR650D
Number of cells in series	90
Number of cells in series per module	6
Nominal Cell Voltage	1.2 V
Cell Operating Voltage Range	1 - 1.5 V
Cell Nominal Capacity	6.5 Ah
Nominal Energy	0.7 kWh
SOC Operating Range	0.4 - 0.7

II. VEHICLE MODEL

A. Vehicle Configuration

The vehicle model used for this paper is a pretransmission parallel HEV model, as shown in Fig. 1. In this model, the hybrid propulsion system consists of a gasoline engine coupled to an automatic transmission through a gear set and a clutch. In addition, an electric machine (motor/generator) is coupled through another gear set to the transmission input shaft. In this paper, both gear sets have been assigned to have unity gear ratios. The transmission output shaft is coupled to a final drive. The electric path of the hybrid propulsion system consists of the electric machine connected to a rechargeable battery. Table I summarizes the specifications of the vehicle and the propulsion system components. In this vehicle configuration, the power demanded by the driver can be provided either by the engine or the electric motor or both. The available control variables are the engine and motor torques as the engine and motor speeds are determined by the vehicle speed.

Autonomie [28] is used to model the different components of the hybrid propulsion system except for the battery. Autonomie is a MATLAB/Simulink simulation package for powertrain and vehicle model development developed by Argonne National Laboratory. Autonomie provides a variety of existing forward-looking powertrain and vehicle models that can support the evaluation of new control functions in a math-based simulation environment. The battery model from Autonomie is replaced by a model described in the following section.

B. Battery Model

Nickel–metal hydride (NiMH) and lithium-ion (Li-ion) batteries are widely used for electric vehicles [29]. NiMH batteries are primarily used in the HEVs, and Li-ion batteries are used for PHEVs and EVs. Both NiMH and Li-ion batteries exhibit a nonlinear resistance to charge and discharge of current, which is a complex function of the depth of discharge (DOD), charge/discharge rate, open-circuit potential, temperature, and so on. The NiMH cell has a metal hydride [MH_x] anode, a nickel hydroxide [$Ni(OH)_{2-y}$] cathode, and an aqueous potassium hydroxide electrolyte. The Li-ion cell typically has an intercalating carbon anode, a lithium metal oxide cathode, and an organic electrolyte with lithium salts. Detailed models describing the mass balance, potential solutions in electrode/electrolyte, interfacial electrochemical kinetics, and thermal balance across the cell sandwich (current collectors, electrodes, and separator filled with electrolyte) are available [30]–[32]. However, those models, though more accurate, are computationally expensive, with robustness issues for use in control simulations. For this paper, we use a computationally efficient model that is able to capture the charge–discharge behavior well to study thermal response of the batteries [31]. We work with a NiMH battery system, but the analysis can be easily extended to a Li-ion battery system. The battery model implemented here is derived from the experimental discharge characteristics of the cell [33]. A sufficient number of discharge curves at different rates (C-rates) is essential to build an accurate model. The discharge current of the battery is normalized against its nominal capacity and expressed as the C-rate. The experimental discharge curves show that for a given capacity, the cell voltage drops as the current density increases. This relation is linearized for an electrochemical cell and given by (1), also referred to as Newman, Tiedemann, and Gu (NTG) model, from [34] and [35]

$$\begin{cases} J = Y(V_p - V_n - U) \\ U = \sum_{i=0}^{N} a_i \theta^i \\ Y = \sum_{i=0}^{M} b_i \theta^i \end{cases} \tag{1}$$

where J is the current density in $\mathrm{A/m^2}$, Y is the effective conductance in $\mathrm{S/m^2}$, $(V_p - V_n)$ is the measured cell voltage in volts, and U is the open-circuit potential of the cell in volts. The effective conductance Y and the open-circuit potential U are represented as a function of the DOD θ. The constants a_i and b_i are fitting parameters that are determined from cell discharge curves for a number of different C-rates.

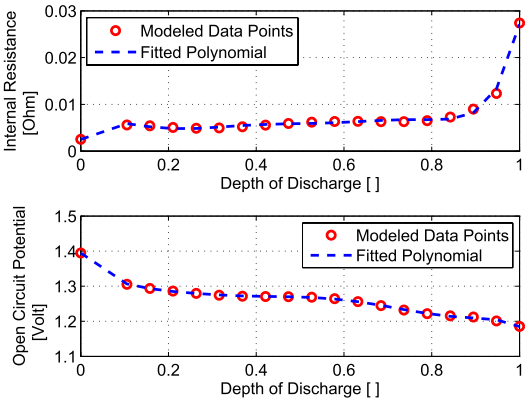

Fig. 2. Variation of the internal resistance and open-circuit potential of the cell as a function of the DOD.

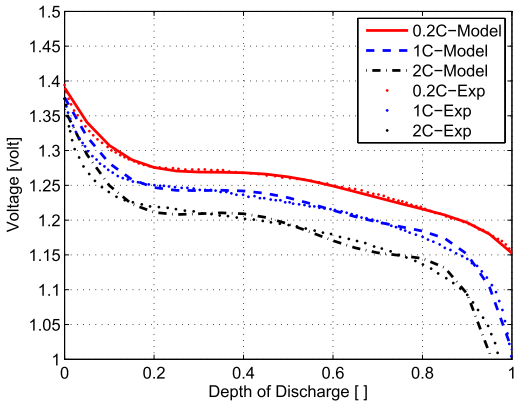

Fig. 3. NiMH battery model validated against the experimental discharge curves at different discharge rates. The 1 C, 2 C, and 0.2 C rates mean that the discharge current will discharge the entire battery in 1, 0.5, and 5 h, respectively.

For different discharge capacities (i.e., DOD θ), it is possible to plot fitted lines representing the linearized relation between the measured cell voltage and current density. The slope of each line represents the reciprocal of the effective conductance Y, while the intercept at zero current density represents the open-circuit potential U. Finally, the variation of Y and U as a function of θ is used to fit the two polynomials described in (1). As a result, for a given value of θ it is possible to calculate the internal resistance $(1/Y)$ and the open-circuit potential U of the cell. Considering the area of the cell, the variation of the internal resistance in ohms and open-circuit potential in volts as a function of the DOD, together with the fitted polynomials are shown in Fig. 2. The model is then validated against the experimental discharge curves at different C-rates, as shown in Fig. 3. This model has been widely used for Li-ion batteries [31], [36]–[38] because of the simplicity of its implementation, its reasonable accuracy, and its low relative computational cost. Subsequently, the calculated internal resistance and open-circuit voltage of the cell at a specific DOD, i.e., SoC $= 1 -$ DOD, are used to compute the rate of SoC change of the battery according to the method described in [39]–[41]. The rate of SoC change of the battery is then used to compute the charge/discharge current I.

The flow of current through the battery leads to internal heat generation due to electrochemical reactions and resistive heating. The amount of generated heat increases the battery temperature, which can be determined through the battery thermal model adopted from [42]. The model considered all the battery internal components as a single homogeneous material with averaged properties. Based on this model, the average temperature increase in the battery, T_{batt}, is a function of the amount of heat generation Q_{gen} and heat loss Q_{loss}, in addition to the thermal mass of the battery and the duration of use

$$T_{\text{batt}} = \int_0^t \frac{Q_{\text{gen}} - Q_{\text{loss}}}{m_{\text{batt}} c_{p,\text{batt}}} dt \tag{2}$$

where m_{batt} is the battery mass, $c_{p,\text{batt}}$ is its heat capacity, and heat generation $Q_{\text{gen}} = J[U - V_p - V_n]$ (here, we have ignored the heat generation due to ohmic losses in current collector and reversible entropic losses). The combination of heat convection (natural or forced) and heat conduction from the battery to the surrounding air is responsible for the determination of the amount of heat retained by the battery (causing the battery temperature to rise). In general, the battery is equipped with a cooling system that starts operation at a specified temperature to prevent the battery from exceeding a high-temperature limit.

Another battery performance characteristic that can be estimated is the final battery range. At each time t, the available energy stored in the battery is estimated based on the current SoC. Considering the conversion efficiency, this amount of stored energy is assumed to be converted to work that moves the vehicle some distance against the total force caused by the vehicle dynamics. The final battery range is then found by calculating the cumulative moving average of the traveled distances over the entire driving cycle. Thus, it indicates the estimated distance that can be traveled based on the driving history using only the available energy in the battery with the engine OFF.

III. Power Management Control Problem

In the rest of this paper, we denote random variables with uppercase letters and their space of realizations by script letters. Subscripts denote time, and subscripts in parenthesis denote a subsystem; for example, $X_{t(j)}$ denotes the random variable of the subsystem j at time t. The shorthand notation $X_{t(1:N)}$ denotes the vector $(X_{t(1)}, X_{t(2)}, \ldots, X_{t(N)})^T$.

A. Problem Formulation

We use a parallel HEV configuration where both the engine and electric motor can provide the power demanded by the driver, either separately or in combination. Because the engine and motor speeds depend on the vehicle speed, the available controllable variables are the engine and motor torques. We consider a state space, $\mathcal{S} \subset \mathbb{R}^n$, for the HEV and a control space, $\mathcal{U} \subset \mathbb{R}^m$, $n, m \in \mathbb{N}$, from which control actions are chosen. In our formulation, the state space is the entire range of the engine and motor speeds, $\mathcal{S} \subset \mathbb{R}^2$, and the control space $\mathcal{U}$ is the vector of engine and motor torques, $\mathcal{U} \subset \mathbb{R}^2$.

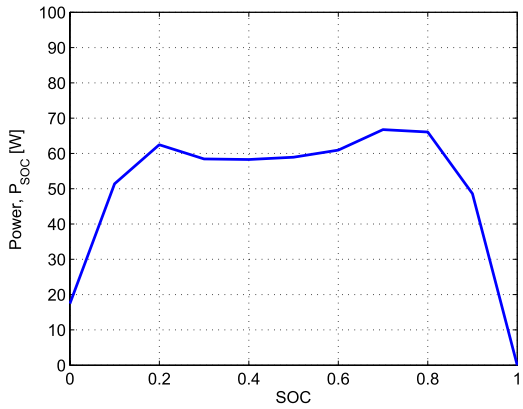

Fig. 4. Maximum charging power for a single cell of the battery with respect to the SoC.

The objective of the power management controller is to guarantee the self-sustainability of the electrical path and distribute the power demanded by the driver optimally between the engine and the motor to maximize HEV efficiency. In most of the work reported in the literature and discussed in Section I, the SoC of the battery has been used as a component of the state. However, this may lead to a significantly large state space with implications for increasing the computational burden associated with solving the problem. In our approach, SoC is correlated to an additional power demand by means of one-on-one mapping. This mapping corresponds to the maximum allowable charging power of the battery P_{SoC} with respect to the SoC. This one-on-one map can be computed as follows:

$$P_{\text{SoC}} = \frac{(V_{\max} - U)V_{\max}}{R} \tag{3}$$

where $V_{\max}$ is the maximum operating cell voltage (i.e., 1.5 V). The open-circuit potential U and the internal resistance R of the cell are polynomial functions of the DOD (i.e., 1 − SoC), as described in Section II and shown in Fig. 2. As a result, the relation between P_{SoC} and SoC is highly dependent on the cell characteristics and design. Fig. 4 shows the maximum allowable charging power for a single cell as given by the battery specifications. At unity SoC, the maximum allowable charging power is set to zero to avoid unnecessary charging of the cell. Thus, based on the current SoC, the mapping indicates the maximum allowable charging power P_{SoC} to be provided to the battery until it reaches the target SoC. This additional amount is added to the driver's power demand, P_{driver}. If SoC is above the target value, then P_{SoC} is assigned to be equal to zero.

The controller observes the engine and motor speeds, and then computes the optimal engine and motor torques, T^*_{eng} and T^*_{mot}, which satisfies the power demanded by the driver, P_{driver}, and the additional amount of power, P_{SoC} that needs to be provided to the battery to stay at the target SoC. The evolution of the state occurs at each time $t = 0, 1, \ldots$, and it is portrayed by the sequence of the random variables $X_{t(1:2)} = (X_{t(1)}, X_{t(2)})^T = (N_{\text{eng}}, N_{\text{mot}})^T \in \mathcal{S}$ and $U_{t(1:2)} = (U_{t(1)}, U_{t(2)})^T = (T_{\text{eng}}, T_{\text{mot}})^T \in \mathcal{U}$, corresponding to the HEV state (engine and motor speeds) and control action (engine and motor torques), respectively. A state-dependent constraint is incorporated in our problem formulation, i.e., for each state $X_{t(1:2)} = i \in \mathcal{S}$ a nonempty set $\mathcal{C}(i) \subset \mathcal{U}$ of admissible control actions (engine and motor torques) is given. The latter implies that at each state $i \in \mathcal{S}$, the control action set $\mathcal{C}(i) \subset \mathcal{U}$ should include only the control actions that satisfy the physical constraints of the engine and the motor.

Definition 1: The set of admissible state/action pairs is defined [43] as

$$\Gamma := \{(X_{t(1:2)}, U_{t(1:2)}) | X_{t(1:2)} = i \in \mathcal{S} \text{ and } U_{t(1:2)} \in \mathcal{C}(i)\}$$

where Γ is the intersection of a closed subset of $\mathbb{R}^2 \times \mathbb{R}^2$ with the set $\mathcal{S} \times \mathcal{U}$.

That is, Γ is closed with respect to the induced topology on $\mathcal{S} \times \mathcal{U}$, and thus it is compact. It follows that for each state $i \in \mathcal{S}$, $\mathcal{C}(i)$ is compact.

Definition 2: The function μ that maps the state space to the control action space, $\mu : \mathcal{S} \to \mathcal{U}$, is defined [43] such that $\mu(i) \in \mathcal{C}(i), \forall i \in \mathcal{S}$.

Let Π be the set of all sequences $\pi = \{\mu(1), \mu(2), \ldots, \mu(|\mathcal{S}|)\}$, where $|\mathcal{S}|$ is the cardinality of the system's state space. Each sequence in Π is called a *stationary control policy* and operates as follows. Associated with each state $i \in \mathcal{S}$ is the function $\mu(i) \in \mathcal{C}(i)$. If at any time the controller finds the system in state i, then the controller always chooses the action based on the function $\mu(i)$. A stationary policy depends on the history of the process only through the current state, and thus to implement it, the controller needs only to know the current state of the system. The advantages for implementation of a stationary policy are apparent as it requires the storage of less information than required to implement a general policy. Thus, a stationary policy is attractive in automotive-related applications, where computational and storage power is limited onboard a vehicle.

At each time t, the controller observes the engine and motor speeds, $X_{t(1:2)} = i \in \mathcal{S}$, which is a function of the vehicle speed, and executes an action, $U_{t(1:2)} = \mu(i)$ (engine and motor torques), from the feasible set of actions, $U_{t(1:2)} \in \mathcal{C}(i)$, at that state. At the same time t, an uncertainty, $W_{t(1:2)}$, is incorporated in the system consisting of the power demanded by the driver, P_{driver}, and the power required by the battery to reach its target value, P_{SoC}. At the next time, $t + 1$, the system transits to the state $X_{t+1(1:2)} = j \in \mathcal{S}$ and a one-stage cost, $k(X_{t(1:2)}, U_{t(1:2)})$, is incurred. This cost can correspond either to a single objective or to a multiobjective optimization criterion, e.g., engine fuel consumption, motor efficiency, and battery capacity and lifetime.

Assumption 1: The one-stage expected cost, $k(X_{t(1:2)}, U_{t(1:2)})$, is continuous and bounded.

After the transition to the next state, a new action is selected and the process is repeated. The state transition from one state to another is imposed by a discrete-time equation that describes the dynamics of the system (HEV) of the form

$$X_{t+1(1:2)} = f_t(X_{t(1:2)}, U_{t(1:2)}, W_{t(1:2)}) \tag{4}$$

where $W_{t(1:2)}$ is the disturbance (driver's power demand, P_{driver} and the power required by the battery to reach its target

value, P_{SoC}) of the HEV at time t. We have full observation of the state of the system, $X_{t(1:2)}$.

Assumption 2: The power demanded by the driver P_{driver} is sequences of independent random variables, independent of the initial state $X_{0(1:2)}$.

Assumption 2 imposes a condition yielding that the state $X_{t+1(1:2)}$ depends only on $X_{t(1:2)}$ and $U_{t(1:2)}$ [44]. Namely, the evolution of the state is a controlled Markov chain and can be represented by a conditional probability, $P(X_{t+1(1:2)} = j | X_{t(1:2)} = i, U_{t(1:2)})$.

The completed period of time over which the system is observed is called the *decision-making horizon* and is denoted by T. The horizon can be either finite or infinite; the infinite decision-making horizon is considered for this problem. This is because we are concerned with deriving an optimal control policy, π, that will optimize the efficiency of the HEV in the long term and not necessarily for a specific period of time. The assumption of an infinite number of decision stages is never satisfied in practice. However, it is a reasonable approximation for problems involving a finite but very large number of stages, e.g., in the HEV power management control problem, where we are interested in optimizing HEV efficiency over the driver's commute.

B. Average Cost Criterion

Infinite horizon problems are interesting as their analysis is insightful, and the implementation of optimal policies is straightforward [45]. The optimal policies are typically stationary as described in the previous section. However, infinite horizon problems require a more sophisticated analysis than finite horizon problems because limiting behavior must be analyzed as the horizon tends to infinity. This is a nontrivial analysis and it can often reveal significant obstacles. There are four principal classes of infinite horizon minimization problems [45]: 1) stochastic shortest path problems; 2) discounted problems with bounded cost per time; 3) discounted and undiscounted problems with unbounded cost per time; and 4) average cost per time problems. For the HEV power management control problem formulated here, we select the average cost criterion as we wish to optimize HEV efficiency with respect to any different commute on average per time. Thus, we are concerned with deriving a stationary optimal control policy π (sequence of engine and motor torques) to minimize the long-run expected average cost per unit time [43]

$$J(\pi) = \min_{\pi \in \Pi} \lim_{T \to \infty} \frac{1}{T+1} \mathbb{E}^{\pi} \left[\sum_{0}^{T} k(X_{t(1:2)}, U_{t(1:2)}) \right]. \quad (5)$$

To guarantee that the limit in (5) exists we impose the following assumption.

Assumption 3: For each stationary control policy $\pi = \{\mu_1, \mu_2, \ldots, \mu_{|\mathcal{S}|}\}$, where $|\mathcal{S}|$ is the cardinality of the system's state space, the Markov chain $\{X_{t(1:2)} | t = 1, 2, \ldots\}$ has a single ergodic class.

That is, for each stationary policy $\pi \in \Pi$ there is a unique probability distribution. In the following section, we discuss how we derive the control policy that minimizes the long-run expected average cost per unit time (5).

IV. Solution of the Power Management Control Problem

A. Multiobjective Optimization Framework

In the HEV configuration adopted here, the engine and the motor are coupled together and their speed is a function of the vehicle speed depending on the gear ratio of the transmission. At each time t, the controller has to optimally split the torque demanded by the driver, T_{driver}, between the engine and motor, T^*_{eng} and T^*_{mot}, to optimize the long-run expected average cost per unit time. The one-stage expected cost, $k(X_{t(1:2)}, U_{t(1:2)})$, in (5) can be either a single objective or multiobjective cost function.

In this section, we formulate the multiobjective optimization framework for the one-stage expected cost that includes fuel consumption, motor efficiency, and battery use and lifetime. Then, we provide the implementation of a power management control algorithm that yields the Pareto efficiency set of the multiobjective problem at each HEV state.

1) Multiobjective Problem Formulation Without the Battery: First, we formulate an optimization problem that considers only the engine and the motor in the one-stage expected cost function. The multiobjective cost consists of the engine's brake specific fuel consumption (BSFC), f_{BSFC}, and the motor's efficiency, η_{mot}. Given the engine and motor speeds which is the pair that constitutes the HEV state $X_{t(1:2)}$, the objective is to find the optimal control action $U_{t(1:2)}$ (engine and motor torques) that minimizes a multiobjective cost function reflecting both the engine's fuel consumption and the motor efficiency. To avoid dominance of one objective function over the other, each function is normalized with respect to its maximum value. Furthermore, since we formulate a minimization problem, we consider the inverse of the motor efficiency.

The BSFC of the engine is a function of the engine speed N_{eng}, and torque, T_{eng}. Similarly, the efficiency of the motor is a function of the motor speed N_{mot} and torque, T_{mot}. Hence, the normalized BSFC of the engine is $f_1(N_{\text{eng}}, T_{\text{eng}}) = (f_{\text{BSFC}}(N_{\text{eng}}, T_{\text{eng}}) / \| f_{\text{BSFC}} \|_\infty)$, where $\| f_{\text{BSFC}} \|_\infty$ corresponds to the maximum engine BSFC value with respect to the entire range of engine speed, N_{eng}, and torque, T_{eng}. The normalized inverse of motor efficiency is $f_2(N_{\text{mot}}, T_{\text{mot}}) = ((1/\eta_{\text{mot}}(N_{\text{mot}}, T_{\text{mot}})) / \|(1/\eta_{\text{mot}})\|_\infty)$, where $\|\eta_{\text{mot}}\|_\infty$ corresponds to the maximum motor efficiency with respect to the entire range of motor speed N_{mot} and torque, T_{mot}.

The multiobjective optimization problem for the one-stage expected cost function is formulated as

$$\begin{aligned} &\min_{U_t} k(X_{t(1:2)}, U_{t(1:2)}) \\ &\quad = \min_{U_t} (\alpha \cdot f_1(X_{t(1)}, U_{t(1)}) + (1-\alpha) \cdot f_2(X_{t(2)}, U_{t(2)})) \\ &\qquad \text{s.t.} \sum_{i=1}^{2} U_{t(i)} = \sum_{i=1}^{2} W_{t(i)} = T_{\text{driver}} + T_{\text{SoC}} \end{aligned} \quad (6)$$

where α is a scalar that takes values in [0, 1], $X_{t(1:2)} = (X_{t(1)}, X_{t(2)})^T = (N_{\text{eng}}, N_{\text{mot}})^T \in \mathcal{S}$, $U_{t(1:2)} = (U_{t(1)}, U_{t(2)})^T = (T_{\text{eng}}, T_{\text{mot}})^T \in \mathcal{U}$ is the vector of engine and motor torques, and T_{SoC} is the torque corresponding to the power required by the battery, P_{SoC}, to reach its target value. Since P_{SoC} is

provided exclusively by the engine, T_{SoC} is computed by dividing P_{SoC} by the engine speed N_{eng}. The multiobjective optimization problem in (6) yields the Pareto efficiency set between the engine and the motor by varying α from 0 to 1 at any given state of the HEV.

2) Multiobjective Problem Formulation With the Battery: Now, we extend the formulation in (6) to include battery lifetime and capacity. The rate of SoC change of the battery with time is considered as an implicit measure for both battery lifetime and capacity. In general, the battery lifetime is strongly affected by the operating temperature which depends mainly on the battery charge/discharge current. On the other hand, the expected range depends mainly on the available energy (capacity) in the battery. Both, current and available energy are profoundly affected by the rate of change of the battery SoC. Hence, for a given SoC value the normalized SoC change, $\Delta\text{SoC} = \text{SoC}(t+1) - \text{SoC}(t)$, of the battery is

$$f_3(N_{\text{mot}}, T_{\text{mot}}) = \frac{|\Delta\text{SoC}|}{\|\Delta\text{SoC}\|_\infty} \tag{7}$$

where $\|\Delta\text{SoC}\|_\infty$ is the maximum SoC change that can occur between a time interval t and $t+1$, and it is computed as follows. The SoC change, ΔSoC, is a function of the SoC and the motor's power at each time t. We use the battery model described in the previous section and compute the SoC change for all possible combinations of the SoC and motor power. Then, $\|\Delta\text{SoC}\|_\infty$ is the maximum from all these values.

The multiobjective optimization problem for the one-stage expected cost function when the engine, motor, and battery are considered, is formulated as

$$\begin{aligned}
&\min_{U_t} k(X_{t(1:2)}, U_{t(1:2)}) \\
&\min_{U_t} (\alpha \cdot f_1(X_{t(1)}, U_{t(1)}) + (1-\alpha)\cdot(\beta \cdot f_2(X_{t(2)}, U_{t(2)}) \\
&\qquad + (1-\beta)\cdot f_3(X_{t(2)}, U_{t(2)}))) \\
&\text{s.t.} \sum_{i=1}^{2} U_{t(i)} = \sum_{i=1}^{2} W_{t(i)} = T_{\text{driver}} + T_{\text{SoC}}
\end{aligned} \tag{8}$$

where α and β are weighting factors changing between 0 and 1. The factor α weights the thermal (e.g., engine) and electrical (e.g., motor and battery) path in the HEV, while the factor β weights the components of the electrical path, i.e., the motor and battery.

B. Pareto Control Policy

The result of the multiobjective optimization problems, (6) and (8), is called Pareto efficiency. In a Pareto efficiency allocation among agents, no one can be made better off without making at least one other agent worse. The following is a formal definition.

Definition 3 [46]: A solution $u^o \in \mathcal{U}$ is called Pareto optimal if there is no $u \in \mathcal{U}$ such that $k(x,u) \leq k(x,u^o)$. If u^o is Pareto optimal, $k(x,u^o)$ is defined as efficient. If $u^1, u^2 \in \mathcal{U}$ and $k(x,u^1) < k(x,u^2)$, we say u^1 dominates u^2 and $k(x,u^1)$ dominates $k(x,u^2)$. The set of all Pareto optimal solutions $u^o \in \mathcal{U}$ is defined as the Pareto set, $\mathcal{U}_{\text{Pareto}}$. The set of all efficient points $k(x,u^o) \in \mathcal{Y}$, where $u^o \in \mathcal{U}_{\text{Pareto}}$, is defined as the efficient set, $\mathcal{Y}_{\text{eff}}$.

Now, the question that arises is whether the Pareto efficiency exists. The following known result provides the conditions for its existence.

Proposition 1 [46]: Let $\Gamma \in \mathbb{R}^l$ be a nonempty and compact set and each component $k(X_{t(j)}, U_{t(j)})\colon \Gamma \to \mathbb{R}$ be lower semicontinuous for all $j = 1, \ldots, l, l \in \mathbb{N}$. Then, the Pareto efficiency is not empty.

In our problem, the set of admissible state/action pairs, Γ, is a nonempty compact space (Definition 1). Furthermore, the engine's normalized BSFC, $f_1(X_{t(1)}, U_{t(1)})$; the inverse of the motor's efficiency, $f_2(X_{t(2)}, U_{t(2)})$; and the normalized SoC change of the battery, $f_3(X_{t(3)}, U_{t(3)})$, are all continuous functions. Consequently, the Pareto efficiency exists and can yield the tradeoffs among the engine, motor, and battery desired for this paper.

Definition 4: The Pareto control policy π^o is defined as the policy that yields the Pareto efficient one-stage expected cost for each subsystem at each state.

For the optimization problem (6), the Pareto control policy is derived as follows. Based on the vehicle speed, the HEV state $i \in \mathcal{S}$, engine and motor speeds, is explicitly specified depending on the gear ratio of the transmission. Thus, for each combination of the vehicle speed and torque demand, we solve (6) offline with α taking values from 0 to 1. The control action, $u^o_{(1:2)} = \mu(i)$, realized by the Pareto control policy is the one that yields the minimum one-stage expected cost in (6) among all values corresponding to different α, namely

$$u^o_{(1:2)} = \arg\min_{U_t \in \mathcal{U}} \left\{ k_{\alpha_1}\left(i, u^{\alpha_1}_{(1:2)}\right), \ldots, k_{\alpha_r}\left(i, u^{\alpha_r}_{(1:2)}\right) \right\}, \quad r \in \mathbb{N} \tag{9}$$

where $u^{\alpha_r}_{(1:2)}$ is the solution of (6) when the scalar is α_r, and $k_{\alpha_r}(i, u^{\alpha_r}_{(1:2)})$ is the corresponding minimum one-stage expected cost for the state $i \in \mathcal{S}$ for α_r. Thus, for each state of the HEV and torque demand we derive the Pareto optimal solution that minimizes (6) and store it in a table. If there are multiple solutions, then one of these solutions is selected randomly.

The torque demand equals to $T_{\text{SoC}} + T_{\text{driver}}$ and it has to be provided by the controlled engine and motor torques $T_{\text{eng}} + T_{\text{mot}}$. The value $T_{\text{SoC}} + T_{\text{driver}}$ is mainly dependent on the driving cycle. To derive the Pareto control policy, which does not depend on a specific driving cycle, the torque demand in the optimization algorithm is generated from all possible combinations of $T_{\text{eng}} + T_{\text{mot}}$, where $0 < T_{\text{eng}} \leq T_{\text{eng,max}}$ and $0 < T_{\text{mot}} \leq T_{\text{mot,max}}$. The Pareto control policy is implemented using the stored table. For any combination of vehicle speed and torque demand, the Pareto control policy interpolates the control values of the table corresponding to the Pareto optimal solution, $u^o_{(1:2)} = \mu(i)$ that minimizes one-stage expected cost (6).

For the optimization problem (8), the Pareto control policy is derived as follows. For each combination of the vehicle speed, SoC, and torque demand, we solve (8) offline with α and β taking values from 0 to 1. The control action, $u^o_{(1:2)} = \mu(i)$, realized by the Pareto control policy is the

one that yields the minimum one-stage expected cost in (8) among all values corresponding to different α for a given β, namely

$$u^o_{(1:2)} = \arg\min_{U_t \in \mathcal{U}} \left\{ k_{\alpha_1,\beta_j}\left(i, u^{\alpha_1,\beta_j}_{(1:2)}\right), \ldots, k_{\alpha_m,\beta_j}\left(i, u^{\alpha_m,\beta_j}_{(1:2)}\right) \right\}, \quad m, j \in \mathbb{N} \tag{10}$$

where $u^{\alpha_m,\beta_j}_{(1:2)}$ is the solution of (8) when the scalars are α_m and β_j, and $k_{\alpha_m,\beta_j}(i, u^{\alpha_m,\beta_j}_{(1:2)})$ is the corresponding minimum one-stage expected cost for the state $i \in \mathcal{S}$ for α_m and β_j.

The weighing factor β is specified depending on consumer needs and preferences. For example, assigning small values to β, is a more conservative approach, resulting in penalizing large deviations, and thus having the battery operating close to the desired SoC. On the other hand, assigning large values to β, puts more emphasis on operating the motor efficiently, and thus significant SoC variations are not penalized. For each state of the HEV, SoC, and torque demand we derive the Pareto optimal solution that minimizes (8) and store it in a table. If there are multiple solutions, then one of these solutions is selected randomly.

As described previously, the Pareto control policy is implemented using the stored table. For any combination of vehicle speed, torque demand, and SoC, the Pareto control policy interpolates the control values of the table corresponding to the Pareto optimal solution, $u^o_{(1:2)} = \mu(i)$ that minimizes one-stage expected cost (8). In [47], it has been shown that under the Assumptions 1 and 3 the Pareto control policy minimizes the average cost criterion.

Lemma 1 [47]: The Pareto control policy π^o minimizes the one-stage expected cost both in (6) and (8).

Proof: For any realization of the state at time t, $X_{t(1:2)} = i \in \mathcal{S}$, let $k^{\pi'}(i, u_{(1:2)})$ and $k^{\pi^o}(i, u^o_{(1:2)})$ be the one-stage expected costs at this state corresponding to any control policy π' and the Pareto control policy π^o, respectively. By Definition 4, at each state, the Pareto control policy, π^o, yields the Pareto optimal solution. By Definition 3, there is no $u_{(1:2)} \in \mathcal{U}$ such that $k^{\pi'}(i, u_{(1:2)}) \leq k^{\pi^o}(i, u^o_{(1:2)})$ for all $\pi' \in \Pi$. Thus, at each realization of the random variable $X_{t(1:2)}$, the Pareto control policy, π^o, minimizes the one-stage expected cost both in (6) and (8). ■

Theorem 1 [47]: The Pareto control policy π^o is the optimal control policy π^* that minimizes the average cost criterion (5).

Proof: Let π^o be the Pareto control policy. From Lemma 1, we have that for each realization of the state $X_{t(1:N)} = i$, $k^{\pi^o}(i, U_{t(1:2)}) \leq k^{\pi'}(i, U_{t(1:2)})$ for any control policy $\pi' \in \Pi$. Since the system's one-stage cost is bounded (Assumption 1), taking the expected average sum from $t = 0$ up to a finite time $T \in \mathbb{N}$ is well defined and finite. Thus

$$\frac{1}{T+1}\mathbb{E}^{\pi}\left[\sum_{t=0}^{T} k^{\pi^o}(X_{t(1:2)}, U_{t(1:2)})\right] \leq \frac{1}{T+1}\mathbb{E}^{\pi}\left[\sum_{t=1}^{T} k^{\pi'}(X_{t(1:2)}, U_{t(1:2)})\right]. \tag{11}$$

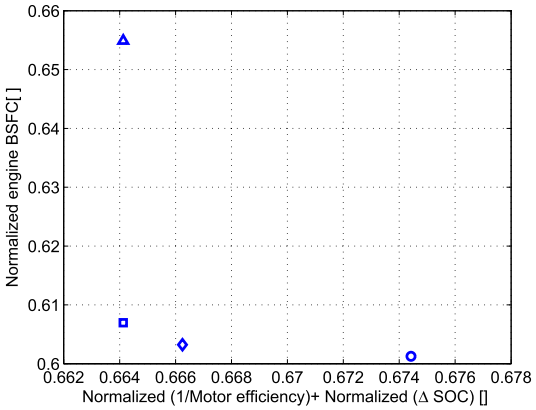

Fig. 5. Pareto efficiency set corresponding to 600 rad/s transmission input shaft speed and 192.4 N·m torque demand.

Taking the lim inf as T goes to infinity

$$\liminf_{T\to\infty} \frac{1}{T+1}\mathbb{E}^{\pi}\left[\sum_{t=0}^{T} k^{\pi^o}(X_{t(1:2)}, U_{t(1:2)})\right] \leq \liminf_{T\to\infty} \frac{1}{T+1}\mathbb{E}^{\pi}\left[\sum_{t=1}^{T} k^{\pi'}(X_{t(1:2)}, U_{t(1:2)})\right]. \tag{12}$$

Since each stationary control policy has a single ergodic class (Assumption 3) the limit in (12) is well defined; hence

$$J^{\pi^o} = \lim_{T\to\infty} \frac{1}{T+1}\mathbb{E}^{\pi}\left[\sum_{t=0}^{T} k^{\pi^o}(X_{t(1:2)}, U_{t(1:2)})\right] \leq J^{\pi'} = \lim_{T\to\infty} \frac{1}{T+1}\mathbb{E}^{\pi}\left[\sum_{t=1}^{T} k^{\pi'}(X_{t(1:2)}, U_{t(1:2)})\right] \ \forall \pi' \in \Pi. \tag{13}$$

■

V. Simulation Results

For our analysis through simulation we used Autonomie [28] modified with the battery model described previously. The vehicle model described in Section II, representing a pretransmission parallel HEV configuration (Fig. 1), was adopted. The speed of the transmission input shaft was determined by the vehicle speed and the operating transmission gear ratio among the five available gear ratios. The torque transmitted through the transmission input shaft was determined by the driver's requested torque, limited by the combined maximum engine and motor torques, in addition to the operating transmission gear ratio. The transmission gear ratio is specified with respect to the vehicle speed and the accelerator pedal position.

To derive the control policy that is Pareto optimal, the multiobjective optimization problem (8) was solved offline for different combinations of SoC, vehicle speed, and torque demand. For each of these different combinations, the Pareto optimal solution was computed and stored in a lookup table. Fig. 5 shows the Pareto efficiency set at 0.6 battery SoC and 600 rad/s transmission input shaft speed when the required

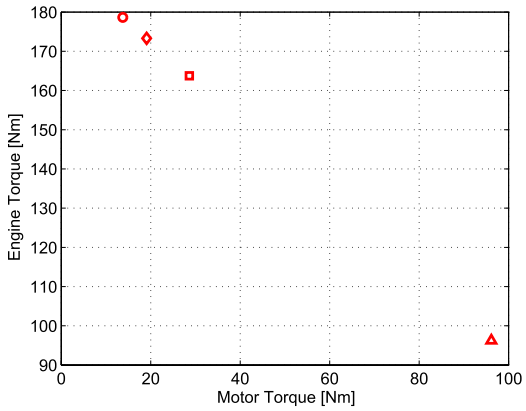

Fig. 6. Pareto set corresponding to 600 rad/s transmission input shaft speed and 192.4 N·m torque demand.

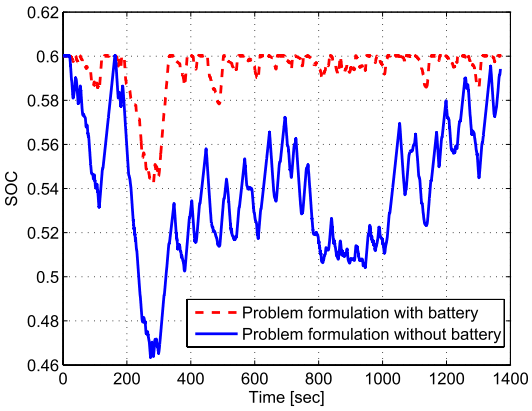

Fig. 7. Comparison of the battery SoC for the problem formulation with and without the battery under the UDDS.

transmission input shaft torque is 192.4 N·m. Fig. 6 shows the set of the corresponding Pareto set, i.e., the optimal combination of engine and motor torques that satisfies the torque demand.

In this particular case, the Pareto optimal solution is $T_{\text{eng}} = 178.6$ and $T_{\text{mot}} = 13.8$ N·m, which yields the normalized engine BSFC, $f_1(x) = 0.6013$, and the normalized combined motor-battery system efficiency when $\beta = 0.5$, e.g., $[0.5 f_2(x) + 0.5 f_3(x)] = 0.6744$. The Pareto control policy can be implemented easily online by interpolating the table of the Pareto optimal solutions with respect to the SoC, vehicle speed, and torque demand. In our analysis, we used thee driving cycles: 1) the urban dynamometer driving schedule (UDDS); 2) the FTP; and 3) the New York, and we compared the Pareto control policy corresponding to the problem formulations (6) and (8), i.e., with and without the battery, to investigate the associated tradeoffs.

A. Driving Cycle Simulation Results

The simulation results using the UDDS driving cycle are presented in this section. Similar trends discussed here were observed in the FTP and New York driving cycles. For both problem formulations the battery was set to operate at a 0.6 target SoC, while subjected to the same cooling rate. For this paper, the cooling system onset temperature was set at 35 °C with a constant air flow rate per module of 20 ft^3/min. The combined power consumed by the cooling system in addition to other accessory systems was estimated to be 200 W.

Fig. 7 shows a comparison of the simulated battery SoC profiles for the two problems, i.e., with and without the battery. It is apparent that considering the battery in the problem formulation in addition to the engine and the motor has a clear impact on the SoC profile. As shown in Fig. 7, the SoC is preserved close to the target value, while the rapid changes in the SoC profile are eliminated. The elimination of the rapid changes in the SoC profile, which is equivalent to the elimination of rapid charging and discharging, directly affects the battery average temperature, as shown in Fig. 8. At the end of the driving cycle, the battery temperature is improved by about 39.3%. Operating the battery close to the

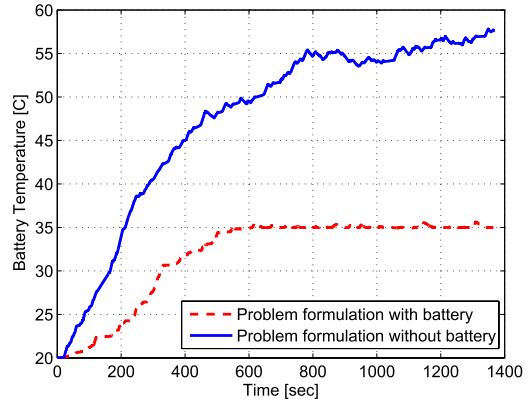

Fig. 8. Comparison of the battery temperature for the problem formulation with and without the battery under the UDDS.

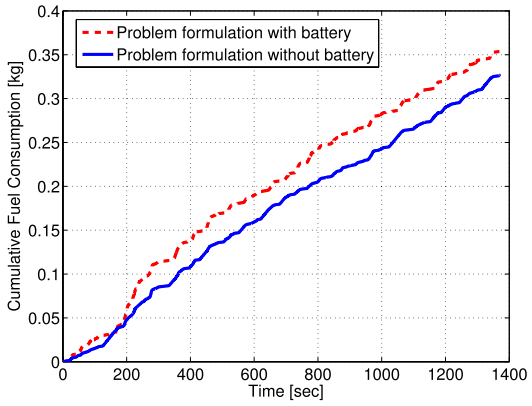

Fig. 9. Comparison of the cumulative fuel consumption for the problem formulation with and without the battery under the UDDS.

onset temperature of the cooling system (35 °C) during the driving cycle, implies the extension of its service life without incurring safety concerns. However, the improvements in the battery performance characteristics comes at the expense of cumulative fuel consumption, as shown in Fig. 9. The cumulative fuel consumption can be found by integrating of the fuel mass consumed at each time t. At the end of the driving cycle, cumulative fuel consumption has increased by about 8.3%.

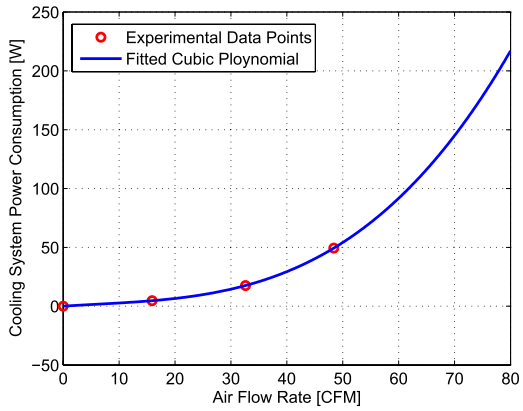

Fig. 10. Power consumption of the cooling system as a function of the battery cooling rate (air flow rate).

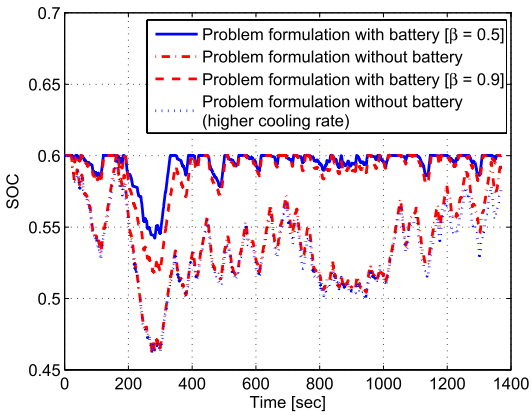

Fig. 11. Effect of increasing the β weighting factor (problem formulation with battery) and applying a higher cooling rate (problem formulation without battery) on the SoC profile for the UDDS.

For the problem formulation with the battery, the weighting factor β in (8) can be used to balance the tradeoffs of fuel consumption and battery performance. On the other hand, if we do not consider the battery in the problem formulation, increasing the battery cooling rate is the direct method to reduce its temperature at the expense of sacrificing significantly fuel consumption. Increasing the battery cooling rate mainly leads to an increase in power consumption. The increase in power consumption by the cooling system as a function of increasing the battery cooling rate can be estimated based on the experimental results provided in [48]. This relationship is shown graphically in Fig. 10, where the hollow circles represent the experimental data points and the solid line represents a fitted cubic polynomial. A detailed investigation and analysis for the tradeoffs between fuel consumption and battery performance is presented in the following sections.

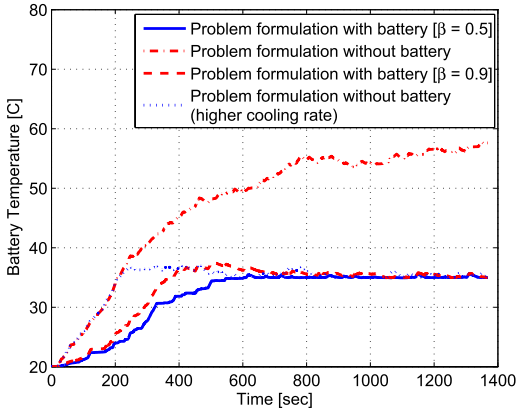

Fig. 12. Effect of increasing the β weighting factor (problem formulation with battery) and applying a higher cooling rate (problem formulation without battery) on the temperature profile for the urban UDDS.

B. Tradeoff Analysis Between the Battery Performance Characteristics and the Cumulative Fuel Consumption

In the analysis presented in the previous section, the β weighting factor in (8) was equal to 0.5, thus weighting the normalized motor efficiency and the normalized SoC change equally. Increasing the β weighting factor will reduce the significance of the normalized SoC rate term in the multiobjective cost function. Consequently, an improvement in the cumulative fuel consumption is expected in the problem formulation with the battery. A slight drop in the SoC profile can be noticed in Fig. 11 when increasing β from 0.5 to 0.9 for the UDDS driving cycle. Relaxing the SoC profile away from the target value leads to a noticeable increase in the battery temperature before the onset of cooling system operation (Fig. 12), as was expected, cumulative fuel consumption drops (by 4.8%), as shown in Fig. 13.

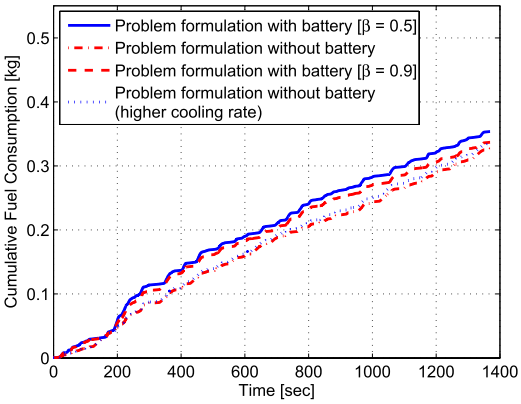

Fig. 13. Effect of increasing the β weighting factor (problem formulation with battery) and applying a higher cooling rate (problem formulation without battery) on the cumulative fuel consumption for the UDDS.

For the problem formulation without the battery, increasing the battery cooling rate mainly leads to an increase in power consumption. In this case, 70 ft^3/min was selected for the cooling rate so that the maximum battery temperature would be as close as possible to that of the problem formulation with the battery. Consequently, it is possible to compare the effect of implementing both problem formulations on the cumulative fuel consumption and the battery estimated range at nearly the same battery temperature. Based on Fig. 10, the increase in power consumption due to increasing the air flow rate from 20 to 70 ft^3/min can be estimated to be about 150 W. As a result, accessory power consumption increased to be 350 W and the SoC profile dropped slightly, as shown in Fig. 11.

TABLE II
RESULTS OF THE TRADEOFF ANALYSIS BETWEEN THE BATTERY PERFORMANCE CHARACTERISTICS AND THE CUMULATIVE FUEL CONSUMPTION AT 60% TARGET SoC

Problem Formulation with Battery [β = 0.5]	
Final Battery Range	1.88 km
Maximum Battery Temperature	35.6 ^{o}C
Cumulative Fuel Consumption	0.354 kg
Problem Formulation with Battery [β = 0.9]	
Final Battery Range	1.85 km
Maximum Battery Temperature	37.5 ^{o}C
Cumulative Fuel Consumption	0.337 kg
Problem Formulation Without Battery	
Final Battery Range	1.67 km
Maximum Battery Temperature	57.8 ^{o}C
Cumulative Fuel Consumption	0.327 kg
Problem Formulation Without Battery with Higher Cooling Rate	
Final Battery Range	1.66 km
Maximum Battery Temperature	37.3 ^{o}C
Cumulative Fuel Consumption	0.334 kg

Apparently, increasing the battery cooling rate leads to a significant drop in the temperature (Fig. 12). At the end of the driving cycle, cumulative fuel consumption increases slightly (about 2.1%), as shown in Fig. 13. Table II summarizes the results of the tradeoff analysis for the different cases.

Some conclusions can be drawn when comparing the results of the problem formulations with the battery at $\beta = 0.9$ and without the battery with higher cooling rate. In both cases, we have nearly the same maximum battery temperature and cumulative fuel consumption. However, the final battery range in the case of the problem formulation with the battery at $\beta = 0.9$ is higher by 11.4% than the other case. Another set of conclusions can be drawn when comparing the results of the problem formulation with the battery at $\beta = 0.9$ and the one without the battery. For the former, the final battery range and the maximum battery temperature are improved by 10.7% and 35.1%, respectively, compared to the latter. However, the improvement of the battery range and temperature has a tradeoff in cumulative fuel consumption of about 3%.

In general, the β weighting factor in the problem formulation with the battery enhances the flexibility of the controller to achieve results comparable with the problem without the battery. In addition, the problem formulation with the battery does not need any additional physical modifications, such as increasing the cooling rate. The effectiveness of this case can be further enhanced through operating the battery at a higher target SoC, as will be discussed in the following section.

C. Operating the Battery at a Higher Target SoC

Considering the battery in the problem formulation (8) allows for controlling battery performance characteristics, such as temperature and range. Consequently, it is possible to operate the battery at a higher target SoC without incurring safety concerns. To show this, the UDDS simulation results using a 0.7 target SoC are shown in Figs. 14–16, which consist of the same four cases described in the previous section. For the problem formulation without the battery, the cooling rate is increased to 80 ft^3/min so that the maximum battery temperature is as close as possible to that of the problem formulation with the battery. Based on Fig. 10, the increase in power consumption resulting from increasing the air mass flow rate from 20 to 80 ft^3/min can be estimated to be about 200 W. As a result, the total accessory power consumption increased to be 400 W.

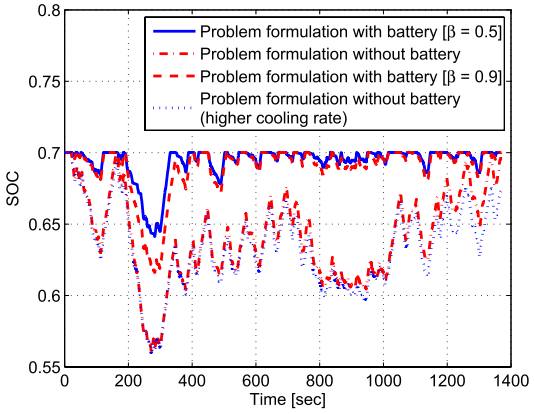

Fig. 14. Effect of increasing the β weighting factor (problem formulation with battery) and applying a higher cooling rate (problem formulation without battery) on the SoC profile for the UDDS at a 70% target SoC.

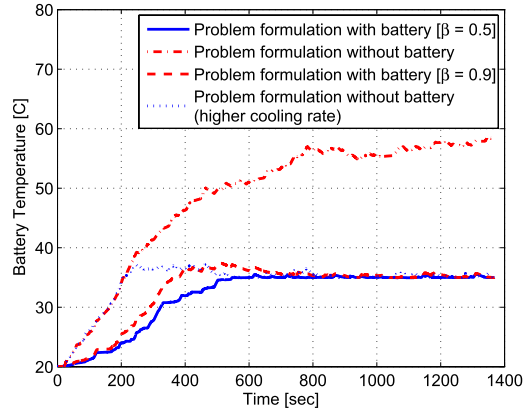

Fig. 15. Effect of increasing the β weighting factor (problem formulation with battery) and applying a higher cooling rate (problem formulation without battery) on the temperature profile for the UDDS at a 70% target SoC.

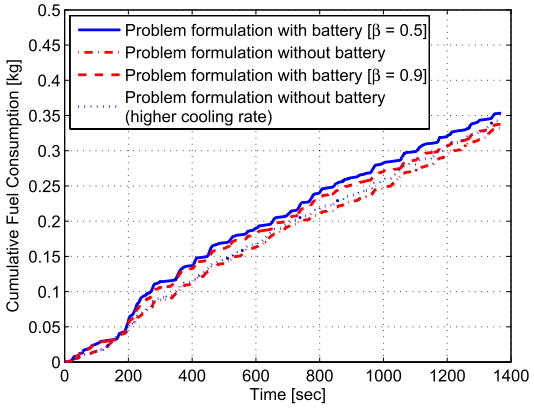

Fig. 16. Effect of increasing the β weighting factor (problem formulation with battery) and applying a higher cooling rate (problem formulation without battery) on the cumulative fuel consumption for the UDDS at a 70% target SoC.

TABLE III
RESULTS OF THE TRADEOFF ANALYSIS BETWEEN THE BATTERY PERFORMANCE CHARACTERISTICS AND THE CUMULATIVE FUEL CONSUMPTION AT 70% TARGET SoC

Problem Formulation with Battery [β = 0.5]	
Final Battery Range	2.35 km
Maximum Battery Temperature	35.6 ^oC
Cumulative Fuel Consumption	0.354 kg
Problem Formulation with Battery [β = 0.9]	
Final Battery Range	2.30 km
Maximum Battery Temperature	37.4 ^oC
Cumulative Fuel Consumption	0.338 kg
Problem Formulation Without Battery	
Final Battery Range	1.96 km
Maximum Battery Temperature	58.7 ^oC
Cumulative Fuel Consumption	0.333 kg
Problem Formulation Without Battery with Higher Cooling Rate	
Final Battery Range	1.94 km
Maximum Battery Temperature	37.3 ^oC
Cumulative Fuel Consumption	0.343 kg

Increasing the β weighting factor from 0.5 to 0.9 in the problem formulation with the battery yields a slight drop in the SoC profile (Fig. 14). Similarly, increasing the cooling rate for the problem formulation without the battery leads to a slight drop in the SoC profile. Apparently, operating at a higher target SoC will lead to an increase in the available energy inside the battery, thus improving the range. For the problem formulation with the battery, increasing the β weighting factor leads to a 2.1% drop in the final battery range. On the other hand, the final battery range is negligibly affected by increasing the cooling rate in the problem without the battery. Increasing the β weighting factor for the problem formulation with the battery leads to a noticeable increase in the battery temperature before the onset of cooling system operation, as shown in Fig. 15. On the other hand, increasing the battery cooling rate for the problem formulation without the battery leads to a significant drop in the temperature, as shown in Fig. 15. Finally, cumulative fuel consumption dropped by 4.4%, as shown in Fig. 16, when the β weighting factor was increased for the problem formulation with the battery. Increasing the battery cooling rate for the problem without the battery leads to a 3.2% increase in cumulative fuel consumption, as shown in Fig. 16.

Table III summarizes the results of the tradeoff analysis for the different cases at a higher target SoC. Some conclusions can be drawn from Table III by comparing the results of the problem formulation with the battery at $\beta = 0.9$ and the problem formulation without the battery with a higher cooling rate. Both cases have nearly the same maximum battery temperature. However, the final battery range and final cumulative fuel consumption in the case of the problem formulation with battery at $\beta = 0.9$ are improved by 18.5% and 1.7%, respectively, than the other case in comparison. Another set of conclusions can be drawn when comparing the results of the problem formulation with battery at $\beta = 0.9$ and the problem formulation without battery. For the problem formulation with battery at $\beta = 0.9$, the final battery range and the maximum battery temperature are improved by 17.3% and 36.2%, respectively, when compared with the problem formulation without battery. However, the improvement in the battery range and temperature has a tradeoff in cumulative fuel consumption of about 1.5%.

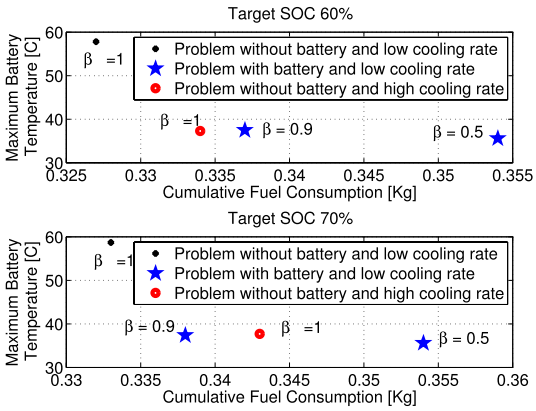

Fig. 17. Tradeoff analysis between the battery performance and cumulative fuel consumption at 60% and 70% target SoC.

The tradeoff analysis between the battery performance characteristics and cumulative fuel consumption for the different solutions of the problem formulation is shown in Fig. 17. As β increases and eventually reaches 1, battery SoC variations are not penalized in the optimization problem formulation (8) with significant implications in battery temperature. However, by decreasing β below 1 or increasing the cooling rate we can still maintain a low battery temperature, and thus improve battery life, with a very small penalty in fuel consumption.

The effect on the simulation results of increasing the target SoC from 60% to 70% can be analyzed by comparing Tables II and III in conjunction with Fig. 17. For the problem formulation with the battery at $\beta = 0.5$ and $\beta = 0.9$, the final battery range increases by 25% and 24.3%, respectively, with negligible change in the maximum battery temperature and cumulative fuel consumption. For the problem formulation without the battery, the final battery range increases by 17.4%. However, the improvement of the battery range has a tradeoff in cumulative fuel consumption of about 1.5% and 1.8%, respectively. For the problem formulation without the battery but at a higher cooling rate, the final battery range increases by 16.8% with negligible change in the maximum battery temperature. Being able to control battery temperature with a penalty in fuel consumption that we feel comfortable with allows us to operate the battery at a higher target SoC without the typical safety concerns associated with temperature increases.

VI. CONCLUSION

The framework proposed in this paper addresses overall HEV optimization, including fuel consumption, motor efficiency, and battery capacity and lifetime. The approach adopted here enhances our understanding of the associated tradeoffs among the HEV subsystems. For instance, the performance of these subsystems can be tailored according to consumer preferences, such as reducing fuel consumption or extending battery life. In addition, the ability to control battery performance indices, such as temperature enables operating the battery at a higher target SoC without incurring

safety concerns. Consequently, the results of such analyses can have significant implications for the related HEV and PHEV ownership and warranty costs.

Ultimately, the proposed optimization framework establishes the foundation for addressing overall HEV optimization, including additional performance characteristics. Thus, paving many pathways for future research work. For instance, reducing the engine emissions can be considered in the multiobjective cost function, thus adding another element to the aforementioned set of consumer preferences. In addition, the proposed framework allows for augmenting the control inputs to include the transmission gearshift schedule as a separate control input, thus enhances the HEV optimal control problem.

REFERENCES

[1] G. Paganelli, M. Tateno, A. Brahma, G. Rizzoni, and Y. Guezennec, "Control development for a hybrid-electric sport-utility vehicle: Strategy, implementation and field test results," in *Proc. Amer. Control Conf.*, vol. 6. 2001, pp. 5064–5069.

[2] A. Sciarretta, M. Back, and L. Guzzella, "Optimal control of parallel hybrid electric vehicles," *IEEE Trans. Control Syst. Technol.*, vol. 12, no. 3, pp. 352–363, May 2004.

[3] C. Musardo, G. Rizzoni, and B. Staccia, "A-ECMS: An adaptive algorithm for hybrid electric vehicle energy management," in *Proc. 44th IEEE Conf. Decision, Control, Eur. Control Conf.*, Dec. 2005, pp. 1816–1823.

[4] F. R. Salmasi, "Control strategies for hybrid electric vehicles: Evolution, classification, comparison, and future trends," *IEEE Trans. Veh. Technol.*, vol. 56, no. 5, pp. 2393–2404, Sep. 2007.

[5] P. Pisu and G. Rizzoni, "A comparative study of supervisory control strategies for hybrid electric vehicles," *IEEE Trans. Control Syst. Technol.*, vol. 15, no. 3, pp. 506–518, May 2007.

[6] C.-C. Lin, H. Peng, J. W. Grizzle, and J.-M. Kang, "Power management strategy for a parallel hybrid electric truck," *IEEE Trans. Control Syst. Technol.*, vol. 11, no. 6, pp. 839–849, Nov. 2003.

[7] O. Sundstrom, L. Guzzella, and P. Soltic, "Torque-assist hybrid electric powertrain sizing: From optimal control towards a sizing law," *IEEE Trans. Control Syst. Technol.*, vol. 18, no. 4, pp. 837–849, Jul. 2010.

[8] C.-C. Lin, H. Peng, and J. W. Grizzle, "A stochastic control strategy for hybrid electric vehicles," in *Proc. Amer. Control Conf.*, vol. 5. Jun./Jul. 2004, pp. 4710–4715.

[9] E. D. Tate, J. W. Grizzle, and H. Peng, "SP-SDP for fuel consumption and tailpipe emissions minimization in an EVT hybrid," *IEEE Trans. Control Syst. Technol.*, vol. 18, no. 3, pp. 673–687, May 2010.

[10] D. F. Opila, X. Wang, R. McGee, R. B. Gillespie, J. A. Cook, and J. W. Grizzle, "An energy management controller to optimally trade off fuel economy and drivability for hybrid vehicles," *IEEE Trans. Control Syst. Technol.*, vol. 20, no. 6, pp. 1490–1505, Nov. 2011.

[11] S. J. Moura, H. K. Fathy, D. S. Callaway, and J. L. Stein, "A stochastic optimal control approach for power management in plug-in hybrid electric vehicles," *IEEE Trans. Control Syst. Technol.*, vol. 19, no. 3, pp. 545–555, May 2011.

[12] H. Borhan, A. Vahidi, A. M. Phillips, M. L. Kuang, I. V. Kolmanovsky, and S. Di Cairano, "MPC-based energy management of a power-split hybrid electric vehicle," *IEEE Trans. Control Syst. Technol.*, vol. 20, no. 3, pp. 593–603, May 2012.

[13] A. A. Malikopoulos, "Stochastic optimal control for series hybrid electric vehicles," in *Proc. Amer. Control Conf.*, Jun. 2013, pp. 1191–1196.

[14] N. A. Chaturvedi, R. Klein, J. Christensen, J. Ahmed, and A. Kojic, "Algorithms for advanced battery-management systems," *IEEE Control Syst.*, vol. 30, no. 3, pp. 49–68, Jun. 2010.

[15] T. Wang and C. G. Cassandras, "Optimal control of multibattery energy-aware systems," *IEEE Trans. Control Syst. Technol.*, vol. 21, no. 5, pp. 1874–1888, Sep. 2013.

[16] T. Wang and C. G. Cassandras, "Optimal control of batteries with fully and partially available rechargeability," *Automatica*, vol. 48, no. 8, pp. 1658–1666, Aug. 2012.

[17] L. Wang, E. G. Collins, Jr., and H. Li, "Optimal design and real-time control for energy management in electric vehicles," *IEEE Trans. Veh. Technol.*, vol. 60, no. 4, pp. 1419–1429, May 2011.

[18] S. J. Moura, D. S. Callaway, H. K. Fathy, and J. L. Stein, "Tradeoffs between battery energy capacity and stochastic optimal power management in plug-in hybrid electric vehicles," *J. Power Sour.*, vol. 195, no. 9, pp. 2979–2988, 2010.

[19] A. A. Malikopoulos, "Impact of component sizing in plug-in hybrid electric vehicles for energy resource and greenhouse emissions reduction," *J. Energy Resour. Technol.*, vol. 135, no. 4, pp. 041201-1–041201-9, 2013.

[20] T.-K. Lee, Y. Kim, D. M. Rizzon, and Z. S. Filipi, "Battery power management in heavy-duty HEVs based on the estimated critical surface charge," *Int. J. Veh. Design*, vol. 61, nos. 1–4, pp. 108–127, 2013.

[21] S. Bashash, S. J. Moura, J. C. Forman, and H. K. Fathy, "Plug-in hybrid electric vehicle charge pattern optimization for energy cost and battery longevity," *J. Power Sour.*, vol. 196, no. 1, pp. 541–549, 2010.

[22] L. Serrao, S. Onori, A. Sciarretta, Y. Guezennec, and G. Rizzoni, "Optimal energy management of hybrid electric vehicles including battery aging," in *Proc. Amer. Control Conf.*, Jun./Jul. 2011, pp. 2125–2130.

[23] S. Ebbesen, P. Elbert, and L. Guzzella, "Battery state-of-health perceptive energy management for hybrid electric vehicles," *IEEE Trans. Veh. Technol.*, vol. 61, no. 7, pp. 2893–2900, Sep. 2012.

[24] A. A. Malikopoulos, "Supervisory power management control algorithms for hybrid electric vehicles: A survey," *IEEE Trans. Intell. Transp. Syst.*, vol. 15, no. 5, pp. 1869–1885, Oct. 2014.

[25] M. Shaltout, A. A. Malikopoulos, S. Pannala, and D. Chen, "Multi-disciplinary decision making and optimization for hybrid electric propulsion systems," in *Proc. IEEE Int. Electr. Veh. Conf.*, Dec. 2014.

[26] P. Ramadass, B. Haran, R. White, and B. N. Popov, "Mathematical modeling of the capacity fade of Li-ion cells," *J. Power Sour.*, vol. 123, no. 2, pp. 230–240, 2003.

[27] G. Ning, R. E. White, and B. N. Popov, "A generalized cycle life model of rechargeable Li-ion batteries," *Electrochim. Acta*, vol. 51, no. 10, pp. 2012–2022, 2006.

[28] *Autonomie*. [Online]. Available: http://www.autonomie.net/, acessed Dec. 4, 2014.

[29] S. M. Lukic, J. Cao, R. C. Bansal, F. Rodriguez, and A. Emadi, "Energy storage systems for automotive applications," *IEEE Trans. Ind. Electron.*, vol. 55, no. 6, pp. 2258–2267, Jun. 2008.

[30] P. Albertus, J. Christensen, and J. Newman, "Modeling side reactions and nonisothermal effects in nickel metal-hydride batteries," *J. Electrochem. Soc.*, vol. 155, no. 1, pp. A48–A60, 2008.

[31] S. Allu, S. Kalnaus, W. Elwasif, S. Simunovic, J. A. Turner, and S. Pannala, "A new open computational framework for highly-resolved coupled three-dimensional multiphysics simulations of Li-ion cells," *J. Power Sour.*, vol. 246, pp. 876–886, Jan. 2014.

[32] P. M. Gomadam, J. W. Weidner, R. A. Dougal, and R. E. White, "Mathematical modeling of lithium-ion and nickel battery systems," *J. Power Sour.*, vol. 110, no. 2, pp. 267–284, 2002.

[33] *Panasonic Nickel Metal Hydride Batteries Handbook*, Panasonic Industrial Europe GmbH, Bracknell Berkshire, U.K., Aug. 2005.

[34] J. Newman and W. Tiedemann, "Potential and current distribution in electrochemical cells," *J. Electrochem. Soc.*, vol. 140, no. 7, pp. 1961–1968, 1993.

[35] H. Gu, "Mathematical analysis of a Zn/NiOOH cell," *J. Electrochem. Soc.*, vol. 130, no. 7, pp. 1459–1464, 1983.

[36] N. Nieto *et al.*, "Thermal modeling of large format lithium-ion cells," *J. Electrochem. Soc.*, vol. 160, no. 2, pp. A212–A217, 2013.

[37] U. S. Kim, J. Yi, C. B. Shin, T. Han, and S. Park, "Modeling the dependence of the discharge behavior of a lithium-ion battery on the environmental temperature," *J. Electrochem. Soc.*, vol. 158, no. 5, pp. A611–A618, 2011.

[38] J. Yi, U. S. Kim, C. B. Shin, T. Han, and S. Park, "Three-dimensional thermal modeling of a lithium-ion battery considering the combined effects of the electrical and thermal contact resistances between current collecting tab and lead wire," *J. Electrochem. Soc.*, vol. 160, no. 3, pp. A437–A443, 2013.

[39] J. Liu and H. Peng, "Control optimization for a power-split hybrid vehicle," in *Proc. Amer. Control Conf.*, Jun. 2006, pp. 466–471.

[40] J. Liu and H. Peng, "Modeling and control of a power-split hybrid vehicle," *IEEE Trans. Control Syst. Technol.*, vol. 16, no. 6, pp. 1242–1251, Nov. 2008.

[41] N. Kim, S. Cha, and H. Peng, "Optimal control of hybrid electric vehicles based on Pontryagin's minimum principle," *IEEE Trans. Control Syst. Technol.*, vol. 19, no. 5, pp. 1279–1287, Sep. 2011.

[42] A. A. Pesaran, "Battery thermal models for hybrid vehicle simulations," *J. Power Sour.*, vol. 110, no. 2, pp. 377–382, 2002.

[43] H. J. Kushner, *Introduction to Stochastic Control*. New York, NY, USA: Holt, Rinehart and Winston, 1971.
[44] A. A. Malikopoulos, "Convergence properties of a computational learning model for unknown Markov chains," *J. Dyn. Syst. Meas. Control*, vol. 131, no. 4, pp. 041011-1–041011-7, 2009.
[45] D. P. Bertsekas, *Dynamic Programming and Optimal Control*, 4th ed. Belmont, MA, USA: Athena Scientific, 2007.
[46] M. Ehrgott, *Multicriteria Optimization*, 2nd ed. New York, NY, USA: Springer-Verlag, 2005.
[47] A. A. Malikopoulos, "A multiobjective optimization framework for online stochastic optimal control in hybrid electric vehicles," *IEEE Trans. Control Syst. Technol.*, 2014.
[48] M. Zolot, A. Pesaran, and M. Mihalic, "Thermal evaluation of Toyota Prius battery pack," SAE Tech. Paper 2002-01-1962, 2002.

Mohamed L. Shaltout (M'14) received the B.Eng. and M.Sc. degrees in mechanical engineering from Cairo University, Giza, Egypt, in 2006 and 2009, respectively. He is currently pursuing the Ph.D. degree with the Department of Mechanical Engineering, University of Texas at Austin, Austin, TX, USA.

He was with the Higher Education Research Experience Program, Oak Ridge National Laboratory, Oak Ridge, TN, USA, in 2013. His current research interests include dynamic systems and controls, with an emphasis on energy systems.

Mr. Shaltout is a member of the American Society of Mechanical Engineers. He received the Fulbright-Egyptian Missions Fellowship from 2011 to 2015, and several awards for academic distinction.

Andreas A. Malikopoulos (M'06) received the Diploma degree in mechanical engineering from the National Technical University of Athens, Athens, Greece, in 2000, and the M.S. and Ph.D. degrees from the Department of Mechanical Engineering, University of Michigan, Ann Arbor, MI, USA, in 2004 and 2008, respectively.

He was a Senior Researcher with General Motors Global Research and Development, Warren, MI, USA, where he is conducting the research in stochastic optimization and control of advanced propulsion systems before joining the Oak Ridge National Laboratory (ORNL), Oak Ridge, TN, USA. He has worked in the industry, where he assigned to major projects focusing on communications systems, commercial telecommunication systems, and command control systems. He is currently the Deputy Director of the Urban Dynamics Institute and an Alvin M. Weinberg Fellow with the Energy and Transportation Science Division, ORNL.

Sreekanth Pannala received the M.S. and Ph.D. degrees in aerospace engineering from the Georgia Institute of Technology, Atlanta, GA, USA, in 1994 and 2000, respectively.

He has served as a Principal Investigator on various Department of Energy (DOE) Computational Science Projects, edited a book entitled *Computational Gas-Solids Flows and Reacting Systems–Theory, Methods and Practice*, and authored over 100 technical publications. He is currently a distinguished research staff member with the Oak Ridge National Laboratory (ORNL), Oak Ridge, TN, USA. He is a Computational Scientist with a broad range of experience in simulating energy processes with primary expertise in the area of developing parallel algorithms and models for heterogeneous chemically reacting flows from device scale to microscale. He is leading a DOE Office of Energy Efficiency and Renewable Energy Project on developing an open-source multiscale/multiphysics framework for designing batteries.

Dr. Pannala was a recipient of the FLC Technology Transfer Award in 2006, the Research and Development 100 Award in 2007, three Significant Event Awards from ORNL, and the Secretary of Energy Achievement Honor Award from Secretary Chu in 2011.

Dongmei Chen (M'09) received the B.S. degree from Tsinghua University, Beijing, China, and the M.S. and Ph.D. degrees in mechanical engineering from the University of Michigan, Ann Arbor, MI, USA.

She is currently an Assistant Professor with the Department of Mechanical Engineering, University of Texas at Austin, Austin, TX, USA. Her current research interests include dynamic systems and controls, in particular, nonminimum phase, multivariable, and mode switching systems, with applications in wind energy, energy storage, and electrical vehicles.

Dr. Chen was a recipient of the CAREER Award from the National Science Foundation in 2011. She received several awards for technical excellence while working in the automotive industry.